Discussion

CrossMark
click for updates

Author for correspondence:
Sara S. Russell
e-mail: sarr@nhm.ac.uk

Heterogeneity in lunar anorthosite meteorites: implications for the lunar magma ocean model

Sara S. Russell[1], Katherine H. Joy[2], Teresa E. Jeffries[1], Guy J. Consolmagno[3] and Anton Kearsley[1]

[1]Natural History Museum, Cromwell Road, London SW7 5BD, UK
[2]School of Earth, Atmospheric and Environmental Sciences, University of Manchester, Manchester M13 9PL, UK
[3]Specola Vaticana, V-00120, Vatican City State

The lunar magma ocean model is a well-established theory of the early evolution of the Moon. By this model, the Moon was initially largely molten and the anorthositic crust that now covers much of the lunar surface directly crystallized from this enormous magma source. We are undertaking a study of the geochemical characteristics of anorthosites from lunar meteorites to test this model. Rare earth and other element abundances have been measured *in situ* in relict anorthosite clasts from two feldspathic lunar meteorites: Dhofar 908 and Dhofar 081. The rare earth elements were present in abundances of approximately 0.1 to approximately $10\times$ chondritic (CI) abundance. Every plagioclase exhibited a positive Eu-anomaly, with Eu abundances of up to approximately $20 \times CI$. Calculations of the melt in equilibrium with anorthite show that it apparently crystallized from a magma that was unfractionated with respect to rare earth elements and ranged in abundance from 8 to $80 \times CI$. Comparisons of our data with other lunar meteorites and Apollo samples suggest that there is notable heterogeneity in the trace element abundances of lunar anorthosites, suggesting these samples did not all crystallize from a common magma source. Compositional and isotopic data from other authors also suggest that lunar anorthosites are chemically heterogeneous and have a wide range of ages. These observations may support other models

Royal Society **Publishing**

of crust formation on the Moon or suggest that there are complexities in the lunar magma ocean scenario to allow for multiple generations of anorthosite formation.

1. Introduction

Remote sensing and geological studies have shown that most of the Moon is covered by a crust of anorthositic rock. Wood *et al.* [1] and Smith *et al.* [2] suggested that this crust formed very early in lunar history, by crystallization of material rich in Ca-rich feldspar from a global magma ocean. By this model, a hot early Moon was mostly or entirely molten. As it cooled, it crystallized first magnesian olivine and then pyroxene, followed by Ca-rich feldspar after about 80% of total crystallization [3–8]. While the mafic minerals are denser than magma and would sink, the feldspar is relatively buoyant and would rise up to form the lunar crust, removing plagiophilic elements from the magma ocean. The timing of this crust formation is model dependent but should occur within about 10 Myr unless it is prolonged by tidal heating [6]. The Apollo suite ferroan anorthosites (FANs) are typically very anorthositic (approx. less than 90% Ca-rich plagioclase: An ~ 95, where plagioclase An = atomic $Ca/(Ca + Na) \times 100$) and are associated with accessory abundances of mafic minerals low-Ca pyroxene, and occasionally clinopyroxene and olivine that have Mg# of around 40–70 (where Mg# = atomic $Mg/(Mg + Fe) \times 100$) [9].

By this model, after plagioclase was removed from the lunar magma ocean melt, Fe-rich and Ti-rich cumulates were precipitated. These mafic cumulates would likely inherit a bulk rock negative Eu-anomaly from the plagioclase-depleted magma, and these types of cumulates would be the source regions of partial melts that subsequently generated mare basalt volcanism. The final material to crystallize from the lunar magma ocean, trapped underneath the anorthositic crust, would be rich in incompatible elements, evidence for this being seen in rocks rich in KREEP (potassium, rare earths and phosphorus).

It is generally thought that after the lunar magma ocean had closed, the Moon underwent a long period of magmatism that emplaced secondary crustal rocks into the pre-existing feldspathic crust (e.g. [4] and references therein). These include the Mg-suite and high alkali suite rock types. The high Mg-suite are typically more mafic rocks (dunites, norites, troctolites and gabbros) compared with FANs. For example, their plagioclase would be more sodic (figure 3) and their associated mafic minerals would have higher Mg numbers (Mg# > 70). They are thought to include mixing with KREEP during their source partial melt or magma ascent process [10]. The alkali suite are typified by containing more sodic plagioclase (An# < 90: figure 3) than other lunar highland lithologies. They are composed of alkali anorthosites, granites, monzogabbros and norites, and, like the Mg-suite rocks, they are KREEP contaminated suggesting that they formed during a secondary stage of lunar magmatism, after the initial formation of the lunar crust.

Geochemical analyses of these types of lunar samples returned by the Apollo missions have greatly increased our understanding of the Moon's geological history (e.g. [4] and references therein). In particular, much information about the early igneous evolution of the Moon has been obtained from abundances and isotopes of trace element abundances, especially for the incompatible rare earth elements (REEs) in lunar crustal samples [11–13]. The REEs in most minerals and bulk rock samples are chemically resilient elements whose distinctive signatures are affected less by metamorphic and metasomatic processing than the more abundant rock-forming elements such as Mg and Fe [12,14–17]. Measurements of these elements have shown that the lunar crustal anorthosites appear to have an overall excess in europium compared with the other REEs, supporting the suggestion that a global magmatic event caused an overall fractionation of trace elements [18]. However, it has also been argued that a simple 'global magma ocean' model cannot account for the diversity of observed major, trace element abundances and isotopic record of anorthite-bearing Apollo samples in detail [19].

We now have a new lunar sample resource—the lunar meteorite collection—that we can use to test models of lunar crust formation [20–23]. Lunar meteorites represent samples of the Moon distinct from those collected by the Apollo or Luna missions. In general, lunar feldspathic meteorites tend to be more anorthosite-rich, and poorer in KREEP, than their Apollo equivalents. For example, Warren *et al.* [24] reported that lunar meteorites tend to have lower incompatible trace element abundances than Apollo samples. The Ni/Ir (as evidence of asteroidal meteoritic addition) of most lunar meteorites is lower than Apollo rocks. As implied by these differences and by evidence from remote sensing compositional data [21,25,26], lunar meteorites almost certainly have sampled different regions of the Moon from those represented by nearside equatorial sample return missions. Indeed, it is very likely that lunar meteorites may have sampled far side highland material more representative of the bulk lunar surface than the nearside regions sampled by the Apollo and Luna missions [15,20,21].

However, lunar meteorites are typically highly impact processed, and deconvolving the chemical and physical effects of impact from primordial signatures is always a challenge. Many lunar meteorites contain anorthositic clasts that may be compositionally pristine [27,28], although there is some debate [29]. These 'relict' clasts are of great interest as they may represent fragments of the ancient anorthositic crust, and so provide information about the crystallites from a primordial lunar magma ocean [1,27,28].
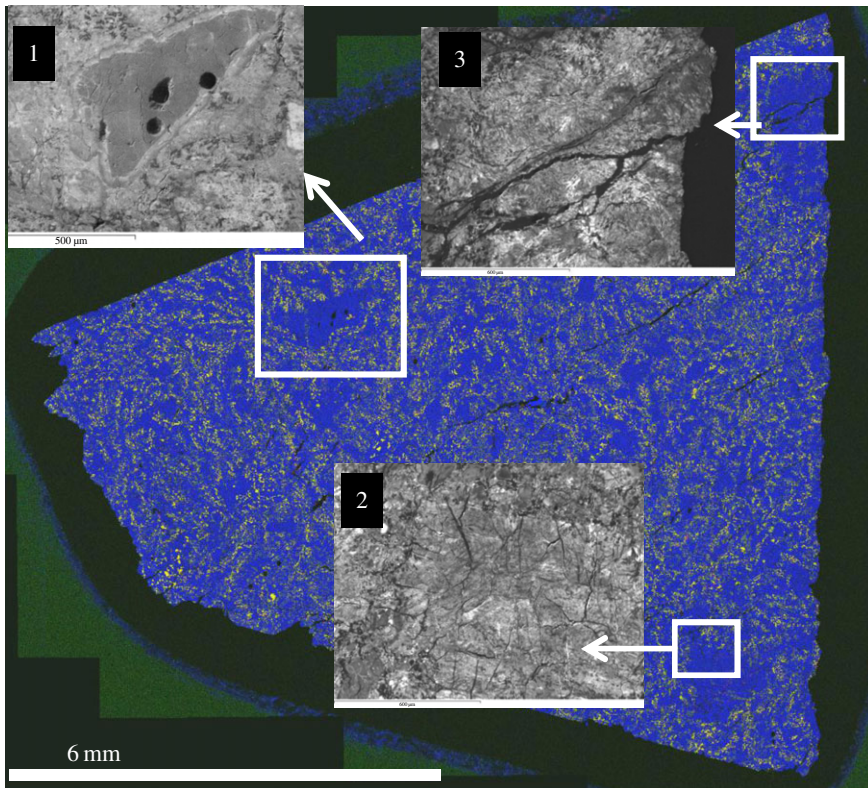
In this paper, we report a study of the petrology and REE composition of clasts from two hot desert feldspathic lunar meteorites, and compare the data with other lunar meteorites and with the Apollo collection. The aim was to determine the original melt composition from which the relict clasts formed. This in turn will allow us to place constraints on the origin and early melting events of the Moon, to assess how these have been affected by later impact processing.

2. Techniques

We studied feldspathic lunar meteorites Dhofar (Dho) 081 and Dho 908. Samples were prepared into 200 μm thick polished sections. For Dho 081, the resin used for section preparation was doped with bismuth, so that accidental analysis of the resin could be easily recognized. The sections were first characterized by reflectance optical microscopy and scanning electron microscopy (SEM; Zeiss EVO 15LS). Samples were imaged using backscattered electron and cathodoluminescence (CL) techniques and energy dispersive X-ray mapping (EDX), to determine whether clast areas were single stoichiometric mineral grains and to document any internal heterogeneity.

Major element abundances were measured by a Cameca SX100 wavelength dispersive electron microprobe at NHM, with a 20 nA beam current, using silicate, oxide and metal standards. Errors (standard deviation in wt%) were Al = 0.11; Si = 0.12; Ca = 0.12; all other elements less than 0.02. Detection limits were less than 250 ppm for each element. Analyses were performed in spot mode using a focused 2 μm beam.

Trace element analyses of relict mineral phases were performed by laser ablation inductively coupled mass spectrometry (LA-ICP-MS). The instrument used was an Agilent 7500cs ICP-MS coupled to an ESI New Wave Research NWR 193 nm laser ablation accessory. Carrier gases were a mix of Ar and He. Analyses were performed *in situ*, using spot analyses with a spatial resolution of approximately 50–100 μm. The size of the analysis volume allows bulk compositional information to be made of individual plagioclase clasts. Measurements were made for 90 s, during which time the abundances of 33 elements were monitored. The external standard used was NIST 612; Ca wt%, as measured by the EMPA was used as an internal standard, by monitoring mass ^{43}Ca and measuring CaO abundance by electron microprobe. Errors for each element are calculated by repeat measurement of NIST 612 standard, typically they are less than 2% (relative standard error). Element determinations are presented as ratios to the Ivuna type carbonaceous chondrite values [30].

Figure 1. SEM-EDX false colour element abundance map of Dhofar 081. Mg = green, Al = blue, Fe = red. The texture indicates that this is an impact melt breccia with melt crystallizing on pristine clasts. CL images of three of the clasts are also shown. Clast 1 appears homogeneous in CL, with a clear reaction rim. All the Dhofar 081 analyses reported from this meteorite in this paper are from this clast. In clast 2, planar features can be seen in CL that are not visible in backscattered electron images. These may be shock-related characteristics. In clast 3, the convoluted schlieren textures seen in CL but not in backscattered electron images suggest that the clast may have remelted.

3. Results

(a) Mineralogy and petrography

Samples. Previous authors have recorded plagioclase major and trace element data from rock and mineral fragments in lunar meteorites MacAlpine Hills (MAC) 88104/05, Dar al Gani (DaG) 262 and 400, Dho 081 [15,31]; see also [32]. We include here additional new data for lunar meteorites Dho 081 and Dho 908.

Dhofar 908 is a granulitic breccia containing magnesian anorthosite-rich lithologies. It has been launch grouped with Dho 489 [33,34] and several other similar stones [31]. It is a dark grey coloured rock containing pinkish to white fragments, composed of rounded lithic clasts within a fine-grained matrix that formed from an impact melt [35]. The weathering grade of this meteorite is fairly high and it contains Ba- and Sr-bearing terrestrial-formed minerals such as celestine.

We studied two sections of Dho 908 (BM 2003 M19): P13288 and P13289, from the collection of the Natural History Museum, London (figure 2). These contained many fine-grained impact melt clasts. Feldspathic clasts are composed of magnesian anorthite, ferran anorthite and fine-grained spinel troctolites. There are also many isolated mineral fragments in the matrix including plagioclase, olivine, pyroxene and troilite. Major element compositions are summarized in table 1.

Table 1. Major element and REE compositions for anorthositic clasts from Dho 081 and Dho 908.

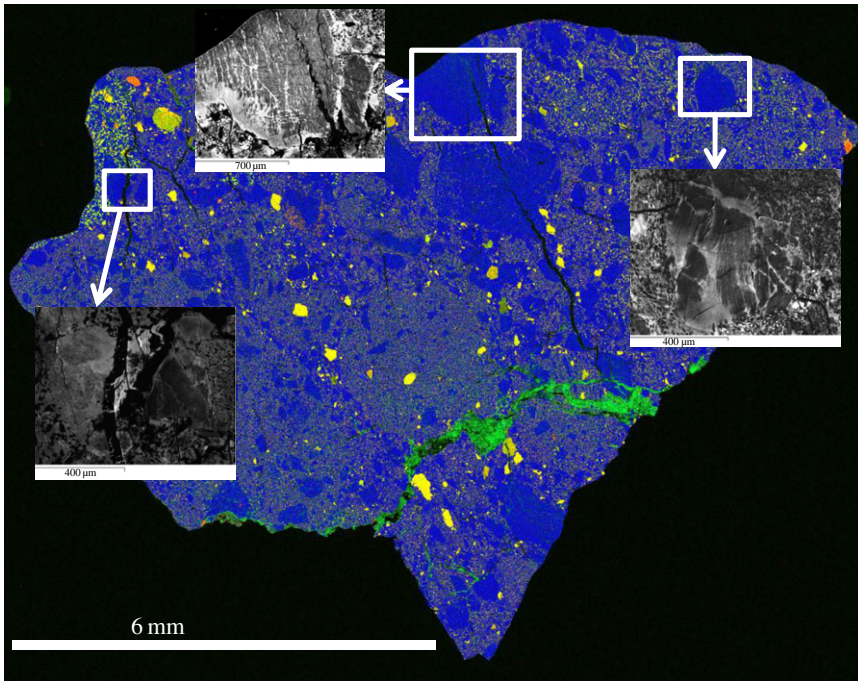|	Dhofar 908 plagioclase												Dhofar 081 plagioclase			
SiO$_2$	43.87	43.87	43.95	43.95	43.94	43.94	43.94	43.27	43.27	43.27	43.39	43.97	44.43	44.43	44.43	44.43
TiO$_2$	0.01	0.01	0.02	0.02	0.02	0.02	0.02	0.00	0.00	0.00	0.08	0.01	0.00	0.00	0.00	0.00
Al$_2$O$_3$	34.63	34.63	34.09	34.09	34.43	34.43	34.43	33.87	33.87	33.87	31.04	34.56	34.96	34.96	34.96	34.96
Cr$_2$O$_3$	0.02	0.02	0.02	0.02	0.02	0.02	0.02	0.01	0.01	0.05	0.02	0.02	0.02	0.02	0.02	0.02
FeO	0.19	0.19	0.53	0.53	0.16	0.16	0.16	0.16	0.16	0.16	1.72	0.46	0.24	0.24	0.24	0.24
MnO	0.00	0.00	0.01	0.01	0.00	0.00	0.00	0.00	0.00	0.00	0.02	0.01	0.00	0.00	0.00	0.00
MgO	0.13	0.13	0.81	0.81	0.17	0.17	0.17	0.26	0.26	0.26	2.87	0.16	0.19	0.19	0.19	0.19
CaO	19.72	19.72	19.48	19.48	19.76	19.76	19.76	19.78	19.78	19.78	18.36	19.92	19.53	19.53	19.53	19.53
CoO	0.00	0.00	0.00	0.00	0.00	0.00	0.00	0.00	0.00	0.00	0.00	0.00	0.01	0.01	0.01	0.01
NiO	b.d.	b.d.	b.d.	b.d.	b.d.	b.d.	b.d.	b.d.	b.d.	b.d.	b.d.	b.d.	0.01	0.01	0.01	0.01
Na$_2$O	0.44	0.44	0.41	0.41	0.45	0.45	0.45	0.41	0.41	0.41	0.36	0.44	0.49	0.49	0.49	0.49
K$_2$O	0.01	0.01	0.01	0.01	0.01	0.01	0.01	0.01	0.01	0.01	0.02	0.03	0.01	0.01	0.01	0.01
total	99.03	99.03	99.33	99.33	98.96	98.96	98.96	97.78	97.78	97.78	97.91	99.59	99.89	99.89	99.89	99.89
Mg#	55.79	55.79	73.39	73.39	64.62	64.62	64.62	73.63	73.63	73.63	74.88	38.64	58.32	58.32	58.32	58.32
Or#	0.05	0.05	0.04	0.04	0.05	0.05	0.05	0.06	0.06	0.06	0.14	0.19	0.07	0.07	0.07	0.07
Ab#	3.91	3.91	3.70	3.70	3.94	3.94	3.94	3.61	3.61	3.61	3.46	3.82	4.33	4.33	4.33	4.33
An#	96.04	96.04	96.26	96.26	96.01	96.01	96.01	96.33	96.33	96.33	96.40	95.99	95.60	95.60	95.60	95.60
LA-ICP-MS#	se02c03	se02c04	se02c05	se02c06	se02c07	se02c08	se02c09	se02c10	se02c11	se02c12	se02c13	se02c15	se02a03	se02a04	se02a05	se02a06
Sc45	2.58 ± 0.019	2.58 ± 0.019	2.07 ± 0.015	2.37 ± 0.017	2.14 ± 0.015	2.37 ± 0.017	2.25 ± 0.015	2.58 ± 0.015	2.15 ± 0.06	2.52 ± 0.018	2.53 ± 0.018	3.09 ± 0.022	3.13 ± 0.036	3.33 ± 0.038	2.82 ± 0.032	3.13 ± 0.036
TiO$_2$ wt%	0.021 ± 0.000	0.019 ± 0.001	0.020 ± 0.001	0.026 ± 0.001	0.012 ± 0.001	0.014 ± 0.001	0.013 ± 0.001	0.02 ± 0.001	0.013 ± 0.001	0.018 ± 0.001	0.046 ± 0.001	0.053 ± 0.001	0.009 ± 0.001	0.008 ± 0.001	0.008 ± 0.001	0.007 ± 0.001
V51	4.67 ± 0.035	6.38 ± 0.048	9.10 ± 0.069	10.60 ± 0.080	6.54 ± 0.050	7.08 ± 0.054	6.43 ± 0.049	4.67 ± 0.051	5.34 ± 0.040	5.32 ± 0.040	5.46 ± 0.041	6.65 ± 0.050	3.37 ± 0.011	3.82 ± 0.012	3.39 ± 0.011	3.47 ± 0.011
MnO wt%	0.005 ± 0.000	0.006 ± 0.001	0.005 ± 0.001	0.006 ± 0.001	0.005 ± 0.001	0.005 ± 0.001	0.005 ± 0.001	0.00 ± 0.000	0.004 ± 0.001	0.007 ± 0.001	0.004 ± 0.001	0.008 ± 0.001	0.004 ± 0.001	0.004 ± 0.001	0.004 ± 0.001	0.005 ± 0.001
Co59	1.60 ± 0.010	1.61 ± 0.010	0.97 ± 0.006	1.98 ± 0.013	0.63 ± 0.004	0.81 ± 0.005	0.75 ± 0.005	1.60 ± 0.004	0.46 ± 0.003	0.87 ± 0.006	0.81 ± 0.005	1.93 ± 0.012	0.23 ± 0.001	0.25 ± 0.001	0.24 ± 0.001	0.21 ± 0.001
Zn64	0.70 ± 0.014	1.26 ± 0.025	6.71 ± 0.135	9.19 ± 0.185	1.96 ± 0.040	1.92 ± 0.039	1.77 ± 0.036	0.70 ± 0.108	2.84 ± 0.057	1.80 ± 0.036	0.93 ± 0.019		0.52 ± 0.004	0.61 ± 0.005	0.52 ± 0.004	0.72 ± 0.006
Ge74	<0.107	<0.111	<0.107	<0.152	<0.158	<0.084	<0.104	<0.107	<0.094	<0.151	<0.186	<0.123	<0.503	<0.746	<0.600	<0.388
Rb85	0.121 ± 0.001	0.132 ± 0.001	0.698 ± 0.004	0.316 ± 0.002	0.111 ± 0.001	0.103 ± 0.001	0.089 ± 0.001	0.121 ± 0.001	0.085 ± 0.001	0.094 ± 0.001	0.389 ± 0.001	0.357 ± 0.002	<0.035	0.089 ± 0.001	<0.028	<0.023
Sr88	311.0 ± 1.0	356.0 ± 1.1	499.0 ± 1.6	409.0 ± 1.3	531.0 ± 1.7	495.0 ± 1.5	382.0 ± 1.2	311.0 ± 6.2	877.0 ± 2.7	339.0 ± 1.1	329.0 ± 1.0	383.0 ± 1.2	168.0 ± 0.9	168.0 ± 0.9	159.0 ± 0.9	166.0 ± 0.9
Y89	0.25 ± 0.003	0.29 ± 0.003	0.29 ± 0.003	0.45 ± 0.005	0.15 ± 0.002	0.15 ± 0.002	0.13 ± 0.002	0.25 ± 0.001	0.18 ± 0.002	0.32 ± 0.004	0.42 ± 0.005	0.83 ± 0.009	0.08 ± 0.001	0.07 ± 0.001	0.06 ± 0.001	0.08 ± 0.001
Zr90	0.20 ± 0.001	0.47 ± 0.002	0.72 ± 0.004	1.17 ± 0.006	0.09 ± 0.000	0.11 ± 0.000	0.11 ± 0.000	0.20 ± 0.001	0.16 ± 0.001	0.13 ± 0.001	0.30 ± 0.002	1.16 ± 0.006	0.14 ± 0.002	0.07 ± 0.001	0.07 ± 0.001	0.07 ± 0.001
Nb93	0.025 ± 0.001	0.036 ± 0.001	0.091 ± 0.004	0.086 ± 0.001	0.013 ± 0.001	0.011 ± 0.001	0.009 ± 0.001	0.011 ± 0.001	0.014 ± 0.001	0.027 ± 0.001	0.027 ± 0.001	0.073 ± 0.000	0.020 ± 0.001	0.020 ± 0.001	0.025 ± 0.000	0.004
Cs133	<0.005	0.004 ± 0.001	0.07 ± 0.001	0.02 ± 0.001	0.00 ± 0.001	<0.004	0.00 ± 0.001	<0.005	0.00 ± 0.001	<0.007	0.01 ± 0.001	0.01 ± 0.001	<0.014	<0.025	<0.011	<0.01
Ba137	237.00 ± 1.885	34.80 ± 0.277	78.70 ± 0.626	81.00 ± 0.644	92.00 ± 0.732	75.80 ± 0.603	60.70 ± 0.483	237.00 ± 1.424	87.30 ± 0.694	60.80 ± 0.484	38.30 ± 0.305	65.20 ± 0.519	6.17 ± 0.042	6.83 ± 0.046	9.28 ± 0.063	6.20 ± 0.042
La139	0.251 ± 0.001	0.258 ± 0.001	0.283 ± 0.002	0.442 ± 0.003	0.05 ± 0.001	0.108 ± 0.001	0.110 ± 0.001	0.251 ± 0.001	0.198 ± 0.001	0.268 ± 0.002	0.349 ± 0.002	0.421 ± 0.002	0.082 ± 0.001	0.055 ± 0.001	0.061 ± 0.001	0.068 ± 0.001
Ce140	0.543 ± 0.004	0.591 ± 0.004	0.607 ± 0.004	1.200 ± 0.008	0.233 ± 0.002	0.254 ± 0.002	0.258 ± 0.002	0.543 ± 0.002	0.499 ± 0.004	0.641 ± 0.005	0.927 ± 0.007	1.120 ± 0.008	0.155 ± 0.001	0.196 ± 0.002	0.151 ± 0.001	0.159 ± 0.001
Pr141	0.073 ± 0.000	0.068 ± 0.000	0.070 ± 0.001	0.134 ± 0.001	0.024 ± 0.001	0.031 ± 0.001	0.031 ± 0.001	0.073 ± 0.001	0.064 ± 0.001	0.074 ± 0.001	0.136 ± 0.001	0.152 ± 0.001	0.025 ± 0.001	0.023 ± 0.001	0.014 ± 0.001	0.026 ± 0.001

(*Continued.*)

Table 1. (*Continued.*)

	Dhofar 908 plagioclase												Dhofar 081 plagioclase			
Nd146	0.325 ± 0.005	0.317 ± 0.005	0.289 ± 0.004	0.547 ± 0.008	0.118 ± 0.002	0.141 ± 0.002	0.141 ± 0.002	0.325 ± 0.002	0.226 ± 0.003	0.348 ± 0.005	0.551 ± 0.008	0.607 ± 0.009	0.160 ± 0.001	<0.159	<0.105	<0.098
Sm147	0.047 ± 0.000	0.070 ± 0.001	0.093 ± 0.001	0.123 ± 0.001	0.039 ± 0.001	0.039 ± 0.001	0.035 ± 0.001	0.047 ± 0.001	0.054 ± 0.001	0.048 ± 0.001	0.150 ± 0.001	0.148 ± 0.001	0.079 ± 0.001			
Eu153	0.750 ± 0.006	0.795 ± 0.006	0.634 ± 0.005	0.635 ± 0.005	0.713 ± 0.006	0.766 ± 0.006	0.751 ± 0.006	0.750 ± 0.005	0.833 ± 0.007	0.897 ± 0.007	0.871 ± 0.007	0.859 ± 0.007	0.832 ± 0.008	0.804 ± 0.008	0.706 ± 0.007	0.703 ± 0.007
Gd157	0.059 ± 0.001	0.079 ± 0.001	0.058 ± 0.001	0.087 ± 0.001	0.030 ± 0.001	0.047 ± 0.001	0.036 ± 0.001	0.059 ± 0.001	0.050 ± 0.001	0.084 ± 0.001	0.137 ± 0.002	0.192 ± 0.003	0.067 ± 0.001	<0.078	<0.062	<0.033
Tb159	0.009 ± 0.001	0.009 ± 0.001	0.009 ± 0.001	0.017 ± 0.001	0.004 ± 0.001	0.005 ± 0.001	0.004 ± 0.001	0.009 ± 0.001	0.006 ± 0.001	0.007 ± 0.001	0.015 ± 0.001	0.026 ± 0.001	<0.011	<0.008	<0.007	<0.006
Dy163	0.047 ± 0.001	0.059 ± 0.001	0.052 ± 0.000	0.105 ± 0.001	0.031 ± 0.001	0.025 ± 0.001	0.024 ± 0.001	0.047 ± 0.001	0.040 ± 0.001	0.054 ± 0.001	0.077 ± 0.001	0.158 ± 0.001	<0.044	<0.033	<0.051	<0.039
Ho165	0.011 ± 0.001	0.010 ± 0.001	0.011 ± 0.001	0.015 ± 0.001	0.004 ± 0.001	0.006 ± 0.001	0.003 ± 0.001	0.011 ± 0.001	0.005 ± 0.001	0.009 ± 0.000	0.015 ± 0.001	0.034 ± 0.001	<0.015	<0.007	<0.008	<0.011
Er166	0.027 ± 0.001	0.021 ± 0.001	0.029 ± 0.001	0.035 ± 0.001	0.018 ± 0.001	0.015 ± 0.001	0.011 ± 0.001	0.027 ± 0.001	0.022 ± 0.001	0.033 ± 0.000	0.049 ± 0.001	0.068 ± 0.001	<0.038	<0.035	<0.058	<0.031
Tm169	<0.002	0.004 ± 0.001	0.004 ± 0.001	0.008 ± 0.001	<0.003	<0.003	0.002 ± 0.001	<0.002	<0.004	0.005 ± 0.001	0.065 ± 0.001	0.011 ± 0.001	0.012 ± 0.001	<0.011	<0.01	<0.01
Yb172	0.025 ± 0.001	0.034 ± 0.001	0.020 ± 0.001	0.045 ± 0.001	0.015 ± 0.001	<0.014	<0.015	0.025	0.030 ± 0.001	0.028 ± 0.001	0.065 ± 0.001	0.068 ± 0.001	0.051 ± 0.001	<0.068	<0.037	<0.065
Lu175	<0.002	0.004 ± 0.001	0.003 ± 0.001	0.007 ± 0.001	0.001 ± 0.001	<0.003	<0.002	<0.002	<0.002	0.004 ± 0.001	0.004 ± 0.001	0.009 ± 0.001	<0.007	<0.015	<0.008	<0.007
Hf178	<0.009	<0.014	0.021 ± 0.001	0.027 ± 0.001	<0.006	<0.016	<0.010	<0.009	<0.012	<0.015	<0.024	0.029 ± 0.001	<0.042	<0.062	<0.038	<0.024
Ta181	<0.002	<0.002	0.005 ± 0.001	<0.003	<0.002	<0.002	<0.002	<0.002	<0.003	<0.003	<0.005	<0.003	<0.012	<0.012	<0.01	<0.009
Pb208	0.104 ± 0.002	0.220 ± 0.003	0.701 ± 0.010	0.921 ± 0.013	0.337 ± 0.005	0.273 ± 0.004	0.264 ± 0.004	0.104 ± 0.008	0.321 ± 0.005	0.151 ± 0.002	0.112 ± 0.002	0.097 ± 0.001	0.097 ± 0.001	<0.038	0.150 ± 0.001	0.090 ± 0.001
Th232	<0.003	0.004 ± 0.001	0.036 ± 0.001	0.028 ± 0.001	<0.002	0.002 ± 0.001	<0.002	<0.003	<0.005	<0.004	0.009 ± 0.001	0.013 ± 0.001	<0.014	<0.013	<0.0001	<0.008
U238	0.072 ± 0.001	0.157 ± 0.001	0.382 ± 0.001	0.384 ± 0.001	0.203 ± 0.001	0.185 ± 0.001	0.202 ± 0.001	0.07 ± 0.001	0.214 ± 0.000	0.155 ± 0.000	0.168 ± 0.001	0.158 ± 0.001	<0.008	<0.011	<0.010	<0.007

equilibrium parent melt CI normalized values lunar plagioclase melt values from [3]

kD																
Sr 1.61	24.8	28.3	39.7	32.6	42.3	39.4	30.4	158.5	69.8	27.0	26.2	30.5	13.4	13.4	12.7	13.2
Ba 0.686	147.6	217	49.0	50.5	57.3	47.2	37.8	111.5	54.4	37.9	23.9	40.6	3.8	4.3	5.8	3.9
La 0.0448	25.6	26.3	28.8	45.0	10.7	11.0	11.2	9.5	20.2	27.3	35.5	42.9	8.4	5.6	6.2	7.0
Ce 0.0302	29.8	32.5	33.3	65.9	12.8	13.9	14.2	12.9	27.4	35.2	50.9	61.5	8.5	10.8	8.3	8.7
Nd 0.0236	30.5	29.7	51.3	51.3	11.1	13.2	14.2	13.2	21.2	32.6	51.7	56.9	15.0			
Sm 0.017	18.7	28.1	37.4	49.2	15.6	15.5	13.9	12.0	21.7	19.2	60.0	59.2	31.7			
Eu 1.2	11.2	11.8	9.4	9.4	10.6	11.4	11.2	10.1	12.4	13.3	13.0	12.8	12.4	12.0	10.5	
Gd 0.0105	28.4	38.4	28.2	41.9	14.5	22.9	17.4	14.9	24.0	40.5	66.2	92.8	32.1			
Dy 0.0089	21.8	27.2	24.0	48.6	14.5	11.5	11.0	9.8	18.3	24.8	73.1					
Er 0.0077	22.0	17.5	23.9	28.4	15.0	12.1	8.6	9.4	17.6	26.6	55.8					
Yb 0.0065	23.4	32.0	19.2	42.2	14.4				28.2	26.6	64.1					

Figure 2. SEM-EDX false colour element abundance map of Dhofar 908. Mg = green, Al = blue, Fe = red. This meteorite is a polymict breccia, more heterogeneous in texture than Dho 081, with large clasts of anorthosite (blue) and spinel-bearing troctolites (yellow). CL images of three of the clasts are also shown. The CL images show that none of the clasts are entirely pristine, but contain patches of less luminescent material that appear to have escaped alteration.

Dhofar 081 is a fragmental breccia with a glass- and melt-rich matrix, brown in colour and abundant vesicles. It is the most Al-rich lunar meteorite as a bulk rock [36]. Clast compositions are diverse and include anorthosite fragments, impact melt breccias and bimineralic fragments [37]. As noted by Cahill *et al.* [15], monolithic-plagioclase clasts are abundant, which are probably relict in origin. Low abundances of Ba and Sr in this meteorite point to a low level of terrestrial contamination [38].

The texture of the section of Dho 081 we studied (BM2004, M5) is that of a clast-bearing impact melt with relict grains that have acted as nucleation sites for crystallization from the surrounding melt (figure 1). There were three large (more than 200 μm) clasts in this section; all are anorthositic in composition. The anorthositic clasts are composed of more than 90% plagioclase (An_{96}) with minor olivine (Fo_{64}) and rare pyroxene. Major element abundances are summarized in table 1.

Warren [29] has warned against interpreting all such small clast sizes as being pristine remnants of crystals from a primary igneous origin. To exclude materials which might have had their bulk composition contaminated by melt processes associated with later impact, we selected only fragments that showed (i) relatively coarse clast size (approx. more than 500 μm), (ii) the presence of pervasive, oriented fracturing indicating crystallinity rather than shock (e.g. maskelynization), (iii) low bulk Mg and Fe abundances suggesting melting of mixed mafic–felsic phases, and (iv) a lack of metal particles derived from impactors. We further began to investigate whether CL could be used to recognize relict clasts, using Dhofar 081 as a case study. We analysed the three main anorthositic clasts in this section by CL. Of these, one seemed homogeneous throughout the interior, and therefore probably pristine (i.e. unshocked) under CL but with a clear reaction rim (figure 1). A second clast showed some planar features that may be related to shock processing and a third showed contorted schlieren textures indicating that this clast had been melted. We conclude that CL may be a useful new tool in documenting textures that can be used to recognize pristine, unshocked, anorthositic clasts in lunar meteorites.

(b) Rare earth element data

(i) Dhofar 081

For Dhofar 081, four analyses were made of the pristine anorthositic clast. REE concentrations are shown in table 1 and in figure 2. The crystals are homogeneous with respect to REE abundances. The light REE abundances (La–Sm) were between 0.2 and 0.5 × chondritic (CI) with little detectable fractionation. Europium showed a clear positive anomaly in all analyses with Eu/Sm of between 5 and 22; its abundance was 12–14 × CI. Heavy REEs (Gd–Lu) were generally below detection levels of the LA-ICP-MS system, but where their abundance could be quantified, they were at levels of around 0.3–0.5 × CI.

(ii) Dhofar 908

In Dhofar 908, 12 measurements of REEs were acquired, on seven separate clasts. REE concentrations are shown in table 1 and in figure 2. Of these, two show clear chemical evidence of terrestrial contamination, as they contain high Sr values of more than 500 ppm compared with 300–400 ppm in the most unaltered plagioclase (table 1). Overall, the data from Dho 908 exhibit a wider variation in REEs than Dho 081. They show a general pattern of being fractionated with an increase in light rare earth element (LREE; 0.2–1.8 × CI), with a clear positive anomaly in Eu (abundance of Eu is 11–16 × CI). Heavy rare earth elements (HREE) are present at levels of 0.06–7 × CI.

(iii) Comparison between meteorites

The single pristine anorthite crystals in Dho 081 fall at the lower end of the range of REE abundances of plagioclase in Dho 908, and it may have less LREE/HREE fractionation than Dho 908.
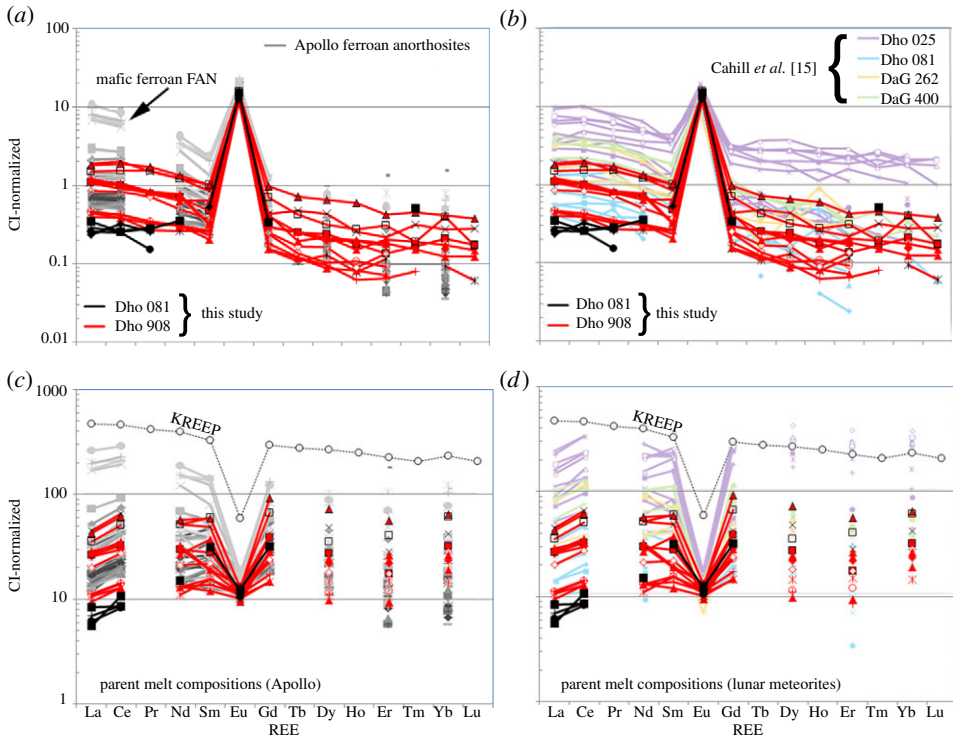
4. Discussion

(a) Comparison to previous work on Apollo and lunar meteorite samples

The lunar highland meteorites discussed here bear major element mineral chemistry similarities to the Apollo FANs. *In situ* analyses of FAN lunar samples by ion microprobe have been performed by Floss *et al.* [39], Jolliff & Hsu [40], Papike *et al.* [41], James *et al.* [42], Snyder *et al.* [43] and Floss *et al.* [12]. Equilibration and redistribution of REEs during metamorphic processes have been carefully considered in these studies. Comparison of REE patterns in coexisting anorthite, olivine and pyroxene shows that extensive redistribution of REEs in plagioclase has not occurred [12,19,41]. (This is also true of most, although not all, coexisting lunar meteorite minerals [15].)
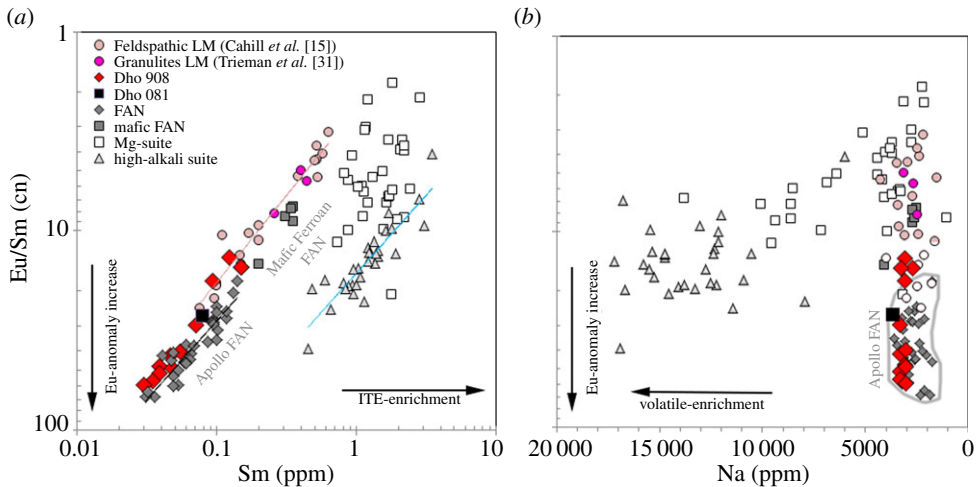
Anorthite crystals in FANs typically exhibit REE abundances at levels of 0.5–10 × CI for LREEs and 0.05–1 × CI for HREEs (figure 3*a*). All anorthites from FANs, and indeed the bulk rocks, show a large positive europium anomaly (figure 3*a,b*), with Eu abundances of around 10 × CI or more. A subset of Apollo FANs, the 'mafic ferroan' FANs [42], have notably higher REE abundances and smaller Eu-anomalies (figure 3*a,b*). Lunar meteorite anorthosites have similar overall REE patterns to Apollo samples (i.e. low REEs and a positive Eu anomaly: figure 3*a*), but there are differences in detail. Anorthite clasts in Dho 081, as measured by our study, have lower LREE abundances than any Apollo FANs.

Joy [32] showed that by plotting Eu/Sm (chondrite normalized showing the degree of the Eu-anomaly) as a function of Sm (as a proxy for the abundance of REEs and other incompatible elements; its abundance in a melt increases as crystallization takes place) and Na (as a proxy for An#), several trends can be distinguished in different Apollo rock types (figure 4). Figure 4 shows the Eu/Sm versus Sm systematics for Apollo samples and lunar meteorites including those from this study.

Figure 3. Chondrite normalized [30] REE patterns for plagioclase in Dhofar 081 and Dhofar 908 compared (*a*) with Apollo FAN samples [12,44] and (*b*) other lunar meteorites [15]. The data and errors are reported in full in table 1. (*c*,*d*) CI-normalized equilibrium parent melts of the same datasets using Kd values of plagioclase compiled by Snyder *et al.* [3]. The composition of KREEP is shown for comparison.

Figure 4. Variations in plagioclase chemistry measured in lunar meteorites (this study, [15,31]) and Apollo highland rock suites [11,12,41,45,46]. Eu/Sm values are chondrite normalized [30] and scale is inverted to reflect Mg# versus An# trends in Apollo highland rock suite mafic and felsic minerals [9]. In (*b*), a field has been drawn around the ferroan anorthosite plagioclase excluding the mafic ferroan group that have lower Eu/Sm ratios.

Anorthite starts to crystallize at around 80% solidification of a parent melt of chondritic composition, and so if this were the starting composition of the lunar magma ocean at time of plagioclase saturation, the anorthite would at first contain REEs at levels of around approximately

$5 \times$ CI (but higher levels of Eu, which is preferentially incorporated into the plagioclase structure). As crystallization progresses, the REE abundances would become higher, as the residual liquid becomes increasingly concentrated in REEs. However, the Eu/Sm would decrease, as more Eu is preferentially scavenged from the melt during plagioclase crystallization. Therefore, a crystallization trend is expected of increasing overall REE and decreasing Eu/Sm.

In figure 4, as crystallization of a homogeneous magma takes place, the composition of crystallizing anorthite would be expected to change along a single straight trend line. This plot shows, however, that the 'mafic ferroan' anorthosites are distinguished from the main group FANs. The high Mg-suite and high alkali suite also clearly have their own chemical trend lines and display heterogeneity within each group, demonstrating a range of source magmas to account for variability at different Apollo landing sites. Analyses of lunar meteorite plagioclase reported in the literature fall on a distinct trend; these rocks typically have smaller Eu-anomalies for their overall REE abundances and high anorthite content [32] (see also figure 4).

The new data we have acquired from Dho 908 span the range for Apollo FANs and lunar anorthosite meteorites. Some analyses in Dho 908 show values similar to the most REE-poor FANs (i.e. the anorthositic ferroan subgroup [12,42]). Other data points have smaller Eu-anomalies similar to other lunar meteorite plagioclase analyses (figures 3 and 4). The data from Dho 081 are limited in this analysis due to low abundances of REEs below the instrument detection limits; however, one data point is intermediate to lunar meteorite and Apollo FAN plagioclase trends.

These data measured in both Apollo FAN plagioclase and lunar meteorite plagioclases, therefore, show a wide range in values and do not fall on a single chemical trend line. This range in petrological and geochemical characteristics of ancient lunar anorthosite must be explained by any model of their formation.

Using mineral-melt element partitioning data, we can estimate the melt composition from which the anorthite crystallized. Most lunar researchers have used the partitioning data compiled by Snyder *et al.* [3]. It has been noted that the Snyder *et al.* partition coefficients may not adequately model the actual REE values in the melt [47]. However, here we are merely comparing differences between Apollo and lunar meteorite anorthosites all calculated using the same set of values; our conclusions remain valid regardless of which set of partition coefficients are used. Furthermore, there is still no consensus in the lunar community about the most appropriate partition coefficients to use for different lunar systems. The Snyder values were used originally for the Apollo data used in many historical petrological models (including those published within the last 5 years), so it avoids confusion to use the same system for Apollo rocks already reported in the literature.

These calculations suggest that the parent melt from which most of the Apollo FAN [12,19,41] formed was unfractionated with respect to REEs, with a small negative Eu-anomaly and divalent REE abundances ranging from 6 to $90 \times$ CI (figure 3). Members of the FAN mafic ferroan suite have higher plagioclase REE (50–$290 \times$ CI: figure 3). According to calculations of Snyder *et al.* [3], if it is assumed that the Moon originally had REEs in chondritic proportions, then the most primitive anorthosites crystallized after approximately 80% of the magma had solidified. At this stage, the melt would be enriched in REEs and other incompatible elements to a degree consistent with that observed in Apollo FANs.

Our calculations of parent melts in equilibrium with clasts from Dho 081 and Dho 908 show a range of compositions, from approximately 6 to approximately $93 \times$ CI and are typically unfractionated. The melt compositions are relatively similar to those observed in most Apollo FANs (figure 3). What is notable is that the Dho 081 plagioclase appears to have crystallized from a more LREE-enriched parent melt than the Apollo FAN samples.

(b) Implications of heterogeneity in crustal anorthosites

The REE data of lunar meteorite and Apollo anorthosites show significant REE (see also [12]) heterogeneity and do not fall on a single trend line in Eu-anomaly (i.e. Eu/Sm chondrite normalized) versus Sm space. We therefore propose that they did not all crystallize from an

initially globally homogeneous but evolving ancient magma ocean. The high level of crystallinity of the global lunar magma when it was close to complete solidification may have caused pockets of melt that were not mixed with the rest of the melt; however, this should not stop them evolving along the same trend as the global composition.

There are other lines of evidence that point to significant differences between lunar anorthosite specimens, also suggesting that they had heterogeneous magma sources.

Gross *et al.* [28] showed that the major element mineral compositions of anorthositic clasts from lunar meteorites do not fit well with the compositional fields as defined by Warren [29] for highland materials. Lunar anorthosites tend to be more magnesian in composition and bridge the gap between FAN and Mg-suite rocks (see also [34,48]). This is also true of the lunar meteorite plagioclase Eu-anomaly (figure 4), which bridges the gap between FANs and Mg-suite rocks. The Mg-rich composition of coexisting mafic minerals is difficult to explain by the lunar magma ocean model, as anorthite crystallizes only after most Mg-rich mafics, and the composition of co-crystallizing mafic minerals would be expected to be more ferroan [28].

Gross *et al.* and also Korotev *et al.* [49] point out that there are no lunar meteorites that are pure anorthosite, merely ones containing anorthositic clasts, weakening the argument that most of the lunar surface contains an underlying anorthosite layer. Furthermore, the lack of KREEP components in most lunar meteorites and measured from remote sensing observations (e.g. [50] and references therein) suggests that KREEP may not be globally distributed in the Moon.

Nyquist *et al.* [27,51] reported Sm–Nd isotope systematics for lunar meteorites and compared these to Apollo rocks. These data show that the εNd of Apollo 16 FAN and lunar meteorites source regions show variations with some samples exhibiting positive εNd and some negative εNd. These data are also supported by those summarized in Borg *et al.* [13,52] and discussed by Longhi [53]. This indicates that they formed from parent magmas both enriched and depleted in the HREEs, whereas an initially chondritic melt would be expected to evolve towards LREE-enriched values as observed in lunar KREEP. The authors concluded that anorthosites do not all form from the same magma source and, therefore, are not all products of the lunar magma ocean.

The ages of lunar anorthosites are reviewed by Carlson *et al.* [54]. The lunar magma ocean theory suggests that anorthosites are the oldest lunar crustal rocks. Age dates for FANs span a range from 4.5 to 4.3 Gyr, but with typically large errors. The most accurate date for a lunar FAN, sample 60025 reported by Borg *et al.* [13] using ^{207}Pb–^{206}Pb, ^{147}Sm–^{143}Nd and ^{146}Sm–^{142}Nd isotopic systems, yields an age of 4360 ± 3 Myr. As this is much later than the formation of the Solar System, the authors concluded that either the Moon formed late (up to 200 Myr after the beginning of the Solar System), or did not have a lunar magma ocean. Indeed, the new ages for measured anorthosites overlap with the ages of lunar basalts and KREEP, in conflict with the magma ocean model. The age of Apollo 16 FAN sample 60025, forming 200 Myr after the beginning of the Solar System, seems too young to be explained as a primary crystallization product of the magma ocean from a Moon that formed approximately 4.5 Gyr ago [55] and produced a plagioclase-rich crust within 10 Myr after formation, unless tidal forces resulted in continued heating [6].

Consolmagno [56] argued that a simple model of magma ocean differentiation and crystallization was incompatible with seismic and other geophysical data. Likewise, recent data from the GRAIL mission [57,58] have led to new estimates of the thickness of the lunar crust of 34–43 km, which are thinner than previously inferred from simple magma ocean models. The GRAIL results, however, are dependent on assumptions about the composition of the lunar crust (they assumed the presence of a lower crust with the density of pure anorthosite) and may have to be revised in light of the geochemical constraints discussed here.

5. Conclusion

The lunar meteorites have enriched and expanded our collection of lunar materials available for study on the Earth. Although heavily impact processed, they can offer additional insights into the geological history of the Moon.

Major and minor element and isotope analyses of lunar meteorites compared to Apollo samples show that the anorthosites did not have a common magma source. This points to a model of their formation that is more complex than crystallization of all anorthosite from a homogeneous lunar magma ocean. One possibility is that a primordial lunar crust formed from a global magma ocean was subjected to secondary anorthositic magmatism. An alternative explanation of crust formation could be through a process of serial magmatism [28,53,59,60], in which plagioclase-rich crystalline mushes formed from large plutons and rose as diapirs to form the lunar crust and were emplaced into a primary lunar magma ocean surface quench crust [53,61]. The more mafic components eventually sank to the mantle, and the crust became increasingly anorthositic. A similar model may explain the origin of terrestrial anorthosites as well [59]. However, the lower gravity of the Moon makes lunar anorthite segregation less efficient than on the Earth.

Alternatively, or in addition to this serial magmatism process, very early (more than 4.3 Ga) impacts of material left over from Solar System formation may have created large-scale regional melting of the 'warm' upper lunar mantle and lunar crust. Plausibly such regional impact melt seas could have differentiated [62–64] giving rise to the large age range of lunar FANs and heterogeneous isotopic and chemical characteristics between Apollo FAN and lunar meteorite feldspathic materials. These alternative models of their formation are also discussed by Crawford & Joy [65] and illustrated in fig. 3 of that work.

Such models are appealing as they allow for heterogeneities in the geochemical characteristics of crustal rocks that are not possible in the magma ocean model, as well as explaining the relatively wide range of ages, and young ages of some lunar anorthosite [13,54]

References

1. Wood JA, Dickey Jr JS, Marvin UB, Powell BN. 1970 Lunar anorthosites. *Science* **167**, 602–604. (doi:10.1126/science.167.3918.602)
2. Smith J, Anderson A, Newton R, Olsen E, Wyllie P, Crewe A, Isaacson M, Johnson D. 1970 Petrologic history of the Moon inferred from petrography, mineralogy, and petrogenesis of Apollo 11 rocks. In *Proc. Apollo 11 Lunar Science Conf.*, vol. 1, pp. 897–925. Houston, TX: Lunar and Planetary Institute.
3. Snyder GA, Taylor LA, Neal CR. 1992 A chemical model for generating the sources of mare basalts: combined equilibrium and fractional crystallization of the lunar magmasphere. *Geochim. Cosmochim. Acta* **56**, 3809–3823. (doi:10.1016/0016-7037(92)90172-F)
4. Shearer CK *et al.* 2006 Thermal and magmatic evolution of the Moon. *Rev. Min. Geochem.* **60**, 365–518. (doi:10.2138/rmg.2006.60.4)
5. Elardo SM, Draper DS, Shearer Jr CK. 2011 Lunar magma ocean crystallization 423 revisited: bulk composition, early cumulate mineralogy, and the source regions of the 424 highlands Mg-suite. *Geochim. Cosmochim. Acta* **75**, 3024–3045. (doi:10.1016/j.gca.2011.02.033)
6. Elkins Tanton L, Burgess S, Yin Q-Z. 2011 The lunar magma ocean: reconciling the solidification process with lunar petrology and geochronology. *Earth Planet. Sci. Lett.* **304**, 326–336. (doi:10.1016/j.epsl.2011.02.004)
7. Elkins-Tanton LT, Bercovici D. 2014 Contraction or expansion of the Moon's crust during magma ocean freezing? *Phil. Trans. R. Soc. A* **372**, 20130240. (doi:10.1098/rsta.2013.0240)
8. Rapp JF, Draper DS. 2013 Can fractional crystallization of a lunar magma ocean produce the lunar crust? In *44th Lunar and Planetary Science Conf.*, abstract no. 2732. Houston, TX: Lunar and Planetary Institute.
9. Warren PH. 1993 A concise compilation of petrologic information on possibly pristine nonmare Moon rocks. *Am. Mineral.* **78**, 360–376.
10. Shearer CK, Papike JJ. 1999 Magmatic evolution of the Moon. *Am. Mineral.* **84**, 1469–1494.

11. Papike JJ, Fowler GW, Shearer CK, Layne GD. 1996 Ion microprobe investigation of plagioclase and orthopyroxene from lunar Mg-suite norites: implications for calculating parental melt REE concentrations and for assessing postcrystallization REE redistribution. *Geochim. Cosmochim. Acta* **60**, 3967–3978. (doi:10.1016/0016-7037(96)00212-8)

12. Floss C, James OB, McGee JJ, Crozaz G. 1998 Lunar ferroan anorthosite petrogenesis: clues from trace element distributions in FAN subgroups. *Geochim. Cosmochim. Acta* **62**, 1255–1283. (doi:10.1016/S0016-7037(98)00031-3)

13. Borg LE, Connelly J, Boyet M, Carlson R. 2011 Chronological evidence that the Moon is either young or did not have a lunar magma ocean. *Nature* **477**, 70–72. (doi:10.1038/nature10328)

14. Schwartz JM, McCallum IS. 1998 Minor elements in plagioclase as indicators of subsolidus processes in lunar and terrestrial rocks. In *29th Lunar and Planetary Science Conf.*, abstract no. 1952. Houston, TX: Lunar and Planetary Institute.

15. Cahill JT, Floss C, Anand M, Taylor LA, Nazarov MA, Cohen BA. 2004 Petrogenesis of lunar highlands meteorites: Dhofar 025, Dhofar 081; Dar al Gani 262, and Dar al Gani 400. *Meteorit. Planet. Sci.* **39**, 503–530. (doi:10.1111/j.1945-5100.2004.tb00916.x)

16. Aigner-Torres M, Blundy J, Ulmer P, Pettke T. 2007 Laser ablation ICPMS study of trace element partitioning between plagioclase and basaltic melts: an experimental approach. *Contrib. Mineral. Petrol.* **153**, 647–667. (doi:10.1007/s00410-006-0168-2)

17. Taylor LA, Liu Y, Peters C, Tompkins S, Isaacson P, Cheek L, Thaisen K. 2009 Lunar magma ocean crust: implications of FeO contents in plagioclase. In *40th Lunar and Planetary Science Conf.*, abstract no. 1304. Houston, TX: Lunar and Planetary Institute.

18. Haskin L, Warren PH. 1991 Lunar chemistry. In *Lunar sourcebook: a user's guide to the Moon* (eds GH Heiken, DT Vaniman, BM French), pp. 357–474. Cambridge, UK: Cambridge University Press.

19. Shearer CK, Floss C. 2000 Evolution of the Moon's mantle and crust as reflected in trace element microbeam studies of lunar magmatism. In *Origin of the Earth and Moon* (eds R Canup, K Righter), pp. 339–359. Tucson, AZ: University of Arizona Press.

20. Palme H, Spettel B, Jochum KH, Dreibus G, Weber H, Weckwerth G, Wänke H, Birschoff A, Stöffler D. 1991 Lunar highland meteorites and the composition of the lunar crust. *Geochim. Cosmochim. Acta* **55**, 3105–3122. (doi:10.1016/0016-7037(91)90476-L)

21. Korotev RL, Jolliff BL, Zeigler RA, Gillis JJ, Haskin LA. 2003 Feldspathic lunar meteorites and their implications for compositional remote sensing of the lunar surface and the composition of the lunar crust. *Geochim. Cosmochim. Acta* **67**, 4895–4923. (doi:10.1016/j.gca.2003.08.001)

22. Korotev RL. 2005 Lunar geochemistry as told by lunar meteorites. *Chemie der Erde* **65**, 297–346. (doi:10.1016/j.chemer.2005.07.001)

23. Joy KH, Arai T. 2013 Lunar meteorites: new insights into the geological history of the Moon. *Astron. Geophys.* **54**, 4.28–4.32.

24. Warren PH, Taylor L, Kallemeyn G, Cohen B, Nazarov MA. 2001 Bulk compositional study of three Dhofar lunar meteorites: enigmatic siderophile element results for Dhofar 026. In *32nd Lunar and Planetary Science Conf.*, abstract no. 2197. Houston, TX: Lunar and Planetary Institute.

25. Warren PH, Ulff-Møller F, Kallemeyn GW. 2005 'New' lunar meteorites: impact melt and regolith breccias and large-scale heterogeneities of the upper lunar crust. *Meteorit. Planet. Sci.* **40**, 989–1014. (doi:10.1111/j.1945-5100.2005.tb00169.x)

26. Joy KH, Crawford IA, Russell SS, Kearsley AT. 2010 Lunar meteorite regolith breccias: an *in situ* study of impact melt composition using LA-ICP-MS and implications for the composition of the lunar crust. *Meteorit. Planet. Sci.* **45**, 917–946. (doi:10.1111/j.1945-5100.2010.01067.x)

27. Nyquist L, Shih C-Y, Reese D, Park J, Bogard DD, Garrison DH, Yamaguchi A. 2010 Lunar crystal history recorded in lunar anorthosites. In *41st Lunar and Planetary Science Conf.*, abstract no. 1383. Houston, TX: Lunar and Planetary Institute.

28. Gross J, Treiman AH, Mercer CN. 2014 Lunar feldspathic meteorites: constraints on the geology of the lunar highlands, and the origin of the lunar crust. *Earth Planet. Sci. Lett.* **388**, 318–328. (doi:10.1016/j.epsl.2013.12.006)

29. Warren PH. 2012 Let's get real: not every lunar rock sample is big enough to be representative for every purpose. In *2nd Conf. on the Lunar Highlands Crust*, abstract no. 9034. Houston, TX: Lunar and Planetary Institute.

30. Anders E, Grevesse N. 1989 Abundances of the elements: meteoritic and solar. *Geochim. Cosmochim. Acta* **53**, 197–214. (doi:10.1016/0016-7037(89)90286-X)

31. Treiman AH, Maloy AK, Shearer Jr CK, Gross J. 2010 Magnesian anorthositic granulites in lunar meteorites Allan Hills A81005 and Dhofar 309: geochemistry and global significance. *Meteorit. Planet. Sci.* **45**, 163–180. (doi:10.1111/j.1945-5100.2010.01014.x)

32. Joy KH. 2013 Trace elements in lunar plagioclase as indicators of source lithology. In *44th Lunar and Planetary Science Conf.*, abstract no. 1033. Houston, TX: Lunar and Planetary Institute.

33. Korotev RL, Zeigler RA, Jolliff BL. 2006 Feldspathic lunar meteorites Pecora Escarpment 02007 and Dhofar 489: contamination of the surface of the lunar highlands by post-basin impacts. *Geochim. Cosmochim. Acta* **70**, 5935–5956. (doi:10.1016/j.gca.2006.09.016)

34. Takeda H, Yamaguchi A, Bogard DD, Karouji Y, Ebihara M, Ohtake M, Saiki K, Arai T. 2006 Magnesian anorthosites and a deep crustal rock from the farside crust of the Moon. *Earth Planet. Sci. Lett.* **247**, 171–184. (doi:10.1016/j.epsl.2006.04.004)

35. Russell SS, Folco L, Grady MM, Zolensky ME, Jones R, Righter K, Zipfel J, Grossman J. 2004 The meteoritical bulletin no. 88. *Meteorit. Planet. Sci.* **39**, A215–A272. (doi:10.1111/j.1945-5100.2004.tb00357.x)

36. Korotev RL. 2012 The Lunar Meteorite List. See http://meteorites.wustl.edu/lunar/moon_meteorites_list_alumina.htm#DHO303.

37. Cahill JT, Taylor LA, Anand M, Patchen A, Nazarov MA. 2002 Mineralogy, petrography, and geochemistry of lunar meteorite Dhofar 081: new developments. In *33rd Lunar and Planetary Science Conf.*, abstract no. 1351. Houston, TX: Lunar and Planetary Institute.

38. Nazarov MA, Demidova SI, Taylor LA. 2003 Trace element chemistry of lunar highland meteorites from Oman. In *34th Lunar and Planetary Science Conf.*, abstract no. 1636. Houston, TX: Lunar and Planetary Institute.

39. Floss C, James OB, McGee JJ, Crozaz G. 1991 Lunar ferroan anorthosites: rare earth element measurements of individual plagioclase and pyroxene grains. In *22nd Lunar and Planetary Science Conf.*, pp. 391–392. Houston, TX: Lunar and Planetary Institute.

40. Jolliff BL, Hsu W. 1996 Geochemical effects of recrystallisation and exsolution of plagioclase of ferroan anorthosite. In *27th Lunar and Planetary Science Conf.*, pp. 611–612. Houston, TX: Lunar and Planetary Institute.

41. Papike JJ, Fowler GW, Shearer CK. 1997 Evolution of the lunar crust: SIMS study of plagioclase from ferroan anorthosites. *Geochim. Cosmochim. Acta* **61**, 2343–2350. (doi:10.1016/S0016-7037(97)00086-0)

42. James OB, Floss C, McGee JJ. 1998 Rare earth element distributions in pyroxenes from a lunar mafi-magnesian ferroan anorthosite. In *29th Lunar and Planetary Science Conf.*, abstract no. 1292. Houston, TX: Lunar and Planetary Institute.

43. Snyder GA, Floss C, Taylor LA. 1998 The origin of ferroan anorthosites and rethinking lunar dogma: ion probe trace element analyses of minerals in Apollo 15 rocks. In *29th Lunar and Planetary Science Conf.*, abstract no. 1133. Houston, TX: Lunar and Planetary Institute.

44. Papike JJ, Ryder G, Shearer CK. 1998 Lunar samples. In *Planetary materials* (ed. JJ Papike), pp. 5-001–5-234. Chantilly, VA: Mineralogical Society of America.

45. Shervais JW, McGee JJ. 1998 Ion and electron microprobe study of Mg suite troctolites, norite, and anorthosites from Apollo 14: evidence for urKREEP assimilation during petrogenesis of Apollo 14 Mg-suite rocks. *Geochim. Cosmochim. Acta* **62**, 3009–3023. (doi:10.1016/S0016-7037(98)00195-1)

46. Shervais JW, McGee JJ. 1999 KREEP cumulates in the western lunar highlands: ion and electron microprobe study of alkali-suite anorthosites and norites from Apollo 12 and 14. *Am. Mineral.* **84**, 806–820.

47. Hui H, Oshrin J, Neal C. 2011 Investigation into the petrogenesis of Apollo 14 high-Al basaltic melts through crystal stratigraphy of plagioclase. *Geochim. Cosmochim. Acta* **75**, 6439–6460. (doi:10.1016/j.gca.2011.08.015)

48. Arai T, Takeda H, Yamaguchi A, Ohtake M. 2008 A new model of lunar crust: asymmetry in crustal composition and evolution. *Earth Planets Space* **60**, 433–444.

49. Korotev RL, Jolliff BL, Zeigler RA. 2010 On the origin of the Moon's feldspathic highlands, pure anorthosite, and the feldspathic lunar meteorites. In *41st Lunar and Planetary Science Conf.*, abstract no. 1533. Houston, TX: Lunar and Planetary Institute.

50. Jolliff BL, Gillis JJ, Haskin LA, Korotev RL, Wieczorek MA. 2000 Major lunar crustal terranes: surface expressions and crust-mantle origins. *J. Geophys. Res.* **105**, 4197–4216. (doi:10.1029/1999JE001103)

51. Nyquist L *et al.* 2006 Feldspathic clasts in Yamato-86032: remnants of the lunar crust with implications for its formation and impact history. *Geochim. Cosmochim. Acta* **70**, 5990–6015. (doi:10.1016/j.gca.2006.07.042)

52. Borg L, Norman M, Nyquist L, Bogard D, Snyder G, Taylor L, Lindstrom M. 1999 Isotopic studies of ferroan anorthosite 62236: a young lunar crustal rock from a light rare-earth-element-depleted source. *Geochim. Cosmochim. Acta* **63**, 2679–2691. (doi:10.1016/S0016-7037(99)00130-1)

53. Longhi J. 2003 A new view of lunar ferroan anorthosites: postmagma ocean petrogenesis. *J. Geophys. Res.* **108**, 5083. (doi:10.1029/2002JE001941)

54. Carlson RW, Borg LE, Gaffney AM, Boyet M. 2014 Rb-Sr, Sm-Nd and Lu-Hf isotope systematics of the lunar Mg-suite: the age of the lunar crust and its relation to the time of Moon formation. *Phil. Trans. R. Soc. A* **372**, 20130246. (doi:10.1098/rsta.2013.0246)

55. Touboul M *et al.* 2007 Late formation and prolonged differentiation of the Moon inferred from W isotopes in lunar metals. *Nature* **450**, 1206–1209. (doi:10.1038/nature06428)

56. Consolmagno GJ. 2003 The composition and evolution of a geophysically reasonable Moon produced by a giant impact. In *34th Lunar and Planetary Science Conf.*, abstract no. 1165. Houston, TX: Lunar and Planetary Institute.

57. Wieczorek MA *et al.* 2013 The crust of the Moon as seen by GRAIL. *Science* **6120**, 671–675. (doi:10.1126/science.1231530)

58. Taylor GJ *et al.* 2013 Revised thickness of the lunar crust from GRAIL data: implications for lunar bulk composition. In *44th Lunar and Planetary Science Conf.*, abstract no. 1783. Houston, TX: Lunar and Planetary Institute.

59. Longhi J, Ashwal L. 1985 Two-stage models for lunar and terrestrial anorthosites: petrogenesis without a magma ocean. *J. Geophys. Res. Solid Earth* **90**, C571–C584. (doi:10.1029/JB090iS02p0C571)

60. Jolliff BL, Haskin LA. 1995 Cogenetic rock fragments from a lunar soil: evidence of a ferroan noritic-anorthosite pluton on the Moon. *Geochim. Cosmochim. Acta* **59**, 2345–2374. (doi:10.1016/0016-7037(95)00110-L)

61. Solomon SC, Longhi J. 1977 Magma oceanography. I. Thermal evolution. In *Proc. 8th Lunar Science Conf., Houston, TX, 14–18 March 1977*, pp. 583–599. Houston, TX: Lunar and Planetary Institute.

62. Wetherill GW. 1976 The role of large bodies in the formation of the Earth and Moon. In *Proc. 7th Lunar and Planetary Science Conf.*, pp. 3245–3257. Houston, TX: Lunar and Planetary Institute.

63. Vaughan WM, Head JW, Wilson L, Hess PC. 2013 Geology and petrology of enormous volumes of impact melt on the Moon: a case study of the Orientale basin impact melt sea. *Icarus* **223**, 749–765. (doi:10.1016/j.icarus.2013.01.017)

64. Hurwitz DM, Kring DA. 2013 Composition and structure of the South Pole-Aitken Basin impact melt sheet. In *44th Lunar and Planetary Science Conf.*, abstract no. 2224. Houston, TX: Lunar and Planetary Institute.

65. Crawford IA, Joy KH. 2014 Lunar exploration: opening a window into the history and evolution of the inner Solar System. *Phil. Trans. R. Soc. A* **372**, 20130315. (doi:10.1098/rsta.2013.0315)